

RADIO SUPERNOVA SN 1998bw AND ITS RELATION TO GRB 980425

Zhi-Yun Li and Roger A. Chevalier

Department of Astronomy, University of Virginia, P.O. Box 3818
 Charlottesville, VA 22903; zl4h@virginia.edu, rac5x@virginia.edu

version: December 2, 2024

ABSTRACT

SN 1998bw is an unusual Type Ic supernova that may be associated with the γ -ray burst GRB 980425. We use a synchrotron self-absorption model for its radio emission to deduce that the synchrotron-emitting gas is expanding into a circumstellar medium of approximately r^{-2} density profile, at a speed comparable to the speed of light. We assume that the efficiencies of production of relativistic electrons and magnetic field are constant through the evolution. The circumstellar density is consistent with that expected around the massive star core thought to be the progenitor of SN 1998bw. The explosion energy in material moving with velocity $> 0.5c$ is $\sim 10^{49} - 3 \times 10^{50}$ ergs, with some preference for the high values. The rise in the radio light curves observed at days $20 - 40$ is inferred to be the result of a rise in the energy of the blast wave by a factor ~ 3 . Interaction with a jump in the ambient density is not consistent with the observed evolution. We infer that the boost in energy is from a shell of matter from the explosion that catches up with the decelerating shock front. Both the high explosion energy and the nature of the energy input to the blast wave are difficult to reconcile with energy input from the shock-accelerated high velocity ejecta from a supernova. The implication is that there is irregular energy input from a central engine, which is the type of model invoked for normal γ -ray bursts. The link between SN 1998bw and GRB 980425 is thus strengthened.

Subject headings: gamma-rays: bursts — radio continuum: stars — supernovae: general — supernovae: individual: SN 1998bw

1. INTRODUCTION

SN 1998bw was discovered in an optical search of the error circle of the gamma-ray burst (GRB) source GRB 980425 (Galama et al. 1998b). The light curve of the supernova indicates an explosion time that is consistent with the time of GRB 980425 and Galama et al. (1998b) place the probability of a chance coincidence of the supernova and GRB at 10^{-4} . The supernova

spectrum implied a Type Ic event, but one with an unusually high luminosity and high material velocities. Modeling of the light curve of SN 1998bw suggested an explosion energy of $(2-3) \times 10^{52}$ ergs (Iwamoto et al. 1998; Woosley, Eastman, & Schmidt 1999), more than an order of magnitude higher than a typical supernova energy. Kulkarni et al. (1998) discovered a variable radio source coincident with the optical supernova. Although a number of Type Ib/c supernovae have been found to be radio sources (Weiler et al. 1999), SN 1998bw was more luminous by $\sim 10^2$ at its peak. The unusual, energetic nature of SN 1998bw would seem to further strengthen its association with GRB 980425. On the other hand, observations with *BeppoSAX* showed a decaying X-ray source in the error box of GRB 980425 not coincident with SN 1998bw (Pian et al. 1999; Galama et al. 1998b). This source might have been the X-ray afterglow of the GRB 980425. The lack of a decaying X-ray afterglow at the position of SN 1998bw is an argument against the association with the GRB because all but one of the others 11 GRBs previously detected by *BeppoSAX* had an X-ray afterglow.

The aim of this paper is to develop a model for RSN (radio supernova) 1998bw and to relate its properties to those of SN 1998bw and GRB 980425. Here, we use the term RSN for radio supernova in order to distinguish the radio event from the optical supernova evolution. Waxman & Loeb (1999) have already modeled RSN 1998bw and proposed that the emission is from a thermal distribution of electrons with a shock velocity of $0.3c$. They use this result to infer that the supernova may be unrelated to GRB 980425. Our model uses a more complete data set and includes a relativistic dynamical model. We reach different conclusions from those of Waxman & Loeb.

The plan of the paper is as follows. The properties of RSN 1998bw are compared to those of other radio supernovae in § 2. In § 3, we present a nonrelativistic model for RSN 1998bw. We assume that a power law electron spectrum is produced in the shock front. We treat dynamical and relativistic effects in § 4 and thus restrict the range of possible models. Approximate scaling laws for the range of models are discussed in § 5. Our model for RSN 1998bw is placed in the context of the properties of SN 1998bw and GRB 980425 in § 6. We present a final discussion and conclusions in § 7.

2. COMPARISON TO RADIO SUPERNOVAE

There is a growing data set on radio supernovae of Types Ib/c and II (Weiler et al. 1998, 1999 and references therein). The overall radio evolution can be described as an early phase when optical depth effects are important followed by a transition to a phase with an optically thin power law spectrum (flux $\propto \nu^{-(p-1)/2}$). The power law index for the electron spectrum, p , has not been observed to vary in individual supernovae, although it does vary in the range 2.1 – 3.2 for the group of radio supernovae (Van Dyk et al. 1994a). The time evolution in the optically thin regime can be described by a power law decrease (flux $\propto t^{-w}$), with w ranging from 0.66 (SN 1980K; Weiler et al. 1992) to 1.6 (SN 1983N).

The evolution of the fluxes from RSN 1998bw (Kulkarni et al. 1998; Wieringa, Kulkarni, & Frail 1999; Fig. 1) and the evolution of the spectral indices (Fig. 2) show that the description of radio supernovae in the optically thin regime roughly applies to RSN 1998bw for ages $t \gtrsim 40$ days. The decline is approximately a power law in time with $w = 1.6$ (see also Iwamoto 1999). The electron spectral index shows some variation but generally is in the range $p = 2.2 - 2.6$. There are deviations from the late power law behavior, but the deviations are comparable to those found in other radio supernovae. SN 1998bw belongs to the class of Type Ib/c supernovae (Galama et al. 1998b) and can be compared to these objects. The parameters for the late evolution of radio supernovae of this type are SN 1983N (Ib): $p = 3.0$, $w = 1.6$; SN 1984L (Ib): $p = 3.0$, $w = 1.5$; SN 1990B (Ic): $p = 3.2$, $w = 1.3$ (Van Dyk et al. 1994a). Radio emission has also been observed from the Type Ic SN 1994I, but the results have not been fully published. Observations at 15 and 88 GHz indicate an optically thin spectral index of $p = 2.8 \pm 0.2$ (Wink 1994). The radio spectrum of RSN 1998bw is flatter than those of other Type Ib/c supernovae and its decline rate is at the high end of those observed.

The previously observed Type Ib/c supernovae have similar radio luminosities, within a factor of 2 – 3. Fig. 3 (based on Fig. 4 of Chevalier 1998) shows the times and peak luminosities at 6 cm of radio supernovae; the Type Ib/c supernovae occupy a small area on this plot. SN 1998bw is extraordinary in that its radio luminosity is $\sim 10^2$ higher than that of the other Type Ib/c supernovae. It remains $\sim 10^2$ stronger than SN 1983N over the full observed period of 250 days. Kulkarni et al. (1998) used the high brightness temperature of the source to argue for relativistic expansion. The straight lines in Fig. 3 are from the theory described in Chevalier (1998) which assumes that optically thick phase of the supernova is due to synchrotron self-absorption. The electron spectrum is assumed to be a power law ($p = 2.5$ in Fig. 3) which extends down to transrelativistic energies. An expression for the radius of the emitting region can then be obtained which depends on the factor $(\text{magnetic energy density}/\text{relativistic electron energy density})^{1/(2p+13)}$. In Fig. 3, the factor is taken to be unity; the weak dependence on the energy density ratio provides justification for the assumption. The total energy in fields and particles goes up if the system is far from equilibrium. The position of SN 1998bw in Fig. 3 is suggestive of relativistic motion, which means that the nonrelativistic theory used for Fig. 3 breaks down.

In addition to its high luminosity, RSN 1998bw is also unusual in its evolution leading to the late power law decline. Fig. 1 shows that the power law decline began at high frequencies (4.80 and 8.64 GHz) on day 12 and continued through day 22. Between days 22 and 32, there was a step increase at these frequencies which raised the level of the power law decay by a factor of ~ 2.2 . This behavior has not been previously observed in the light curves of radio supernovae, although SN 1987A has shown a strong rise in its radio flux (Ball et al. 1995) which can be attributed to interaction with the dense wind from a previous evolutionary phase. The observed light curves generally do show fluctuations about smooth curves (Weiler et al. 1999) similar to that seen in the late power law evolution of RSN 1998bw. The radio data on many supernovae are fragmentary, but there are excellent data at 5 frequencies on SN 1993J (Van Dyk et al. 1994b; Weiler et al.

1999). The radio evolution is smooth and can be modeled by shock-accelerated supernova ejecta running into a $\rho \propto r^{-2}$ circumstellar medium (Fransson & Björnsson 1998). Another anomaly in the early evolution of RSN 1998bw is the rise at 4.80 and 8.64 GHz before day 10. The rise occurs with little change in spectral index, which implies that it is not due to a reduction in optical depth, as is the case in other radio supernovae.

3. A MODEL FOR RSN 1998bw

The properties of RSN 1998bw sufficiently resemble those of other radio supernovae to initially consider a model similar to those applied to radio supernovae. The standard model for these objects involves synchrotron emission from relativistic electrons in a spherical shocked region between the supernova and a surrounding circumstellar wind (Chevalier 1982). The early optically thick phase can be dominated by either free-free absorption or synchrotron self-absorption, but the high velocities and low circumstellar densities found in Type Ib/c supernovae implies that synchrotron self-absorption is the dominant mechanism in these objects (Slysh 1990; Chevalier 1998). The same arguments apply to the Type Ic RSN 1998bw (see also Kulkarni et al. 1998). A significant new feature for RSN 1998bw is that the high shock velocity inferred for this radio supernova implies that all the postshock electrons are accelerated to relativistic energies. As in studies of GRB afterglows (Waxman 1997; Wijers, Rees, & Mészáros 1997), we assume that the distribution of relativistic electrons with the Lorentz factor γ takes a power law form with the number density given by

$$n(\gamma) d\gamma = C \gamma^{-p} d\gamma, \quad (1)$$

above a lower limit γ_m , which is determined by the shock velocity. Support for the assumption in the GRB case can be found in the afterglow emission from GRB 970508 (Galama et al. 1998a). This distribution function distinguishes our model for RSN 1998bw from that of Waxman & Loeb (1999), who assumed a thermal (essentially monoenergetic) electron distribution.

Relativistic electrons moving with a Lorentz factor of γ emit synchrotron radiation of a characteristic frequency

$$\nu_c(\gamma) = \frac{3\gamma^2 q B_\perp}{4\pi m c}, \quad (2)$$

where q and m are the charge and the mass of the electron, and B_\perp the strength of the component of magnetic field perpendicular to the electron velocity. In the simplest case where the frequency of interest $\nu \gg \nu_m = \nu_c(\gamma_m)$, the synchrotron spectrum has a $\nu^{5/2}$ spectral dependence in the optically thick region and a $\nu^{-(p-1)/2}$ dependence in the optically thin region (e.g., Rybicki & Lightman 1979). This simple model spectrum fails to reproduce two properties of the observed radio spectrum: (1) at the earliest times when the radio emission is most probably optically thick at the two highest frequencies (3 cm and 6 cm), the spectral index between them is closer to 2 than to 5/2, as noted by Kulkarni et al. (1998) and Waxman & Loeb (1999); and (2) the observed spectrum is significantly broader than the above simple spectrum. These two discrepancies lead

us to believe that the characteristic frequency ν_m is important in shaping the observed spectrum. We explore this possibility and try to infer the physical properties of the radio emitting plasma from ν_m and other parameters that determine the spectrum.

In this section, we restrict our discussion to emission from a nonrelativistically moving medium. It is well known that, in a synchrotron self-absorption model, the flux at a given frequency ν is proportional to

$$f_\nu \propto \nu^{5/2} (1 - e^{-\tau}) \frac{\int_0^{x_m} F(x) x^{(p-3)/2} dx}{\int_0^{x_m} F(x) x^{(p-2)/2} dx}, \quad (3)$$

where $x_m = \nu/\nu_m$, $F(x)$ is a known function of x (shown, e.g., on page 179 of Rybicki & Lightman 1979), and τ is the optical depth of synchrotron self-absorption. From the standard theory, we have

$$\tau \propto \nu^{-(2+p/2)} \int_0^{x_m} F(x) x^{(p-2)/2} dx. \quad (4)$$

To simplify expressions, we define two auxiliary functions

$$F_1(\nu, \nu_m, p) = \int_0^{x_m} F(x) x^{(p-3)/2} dx; \quad F_2(\nu, \nu_m, p) = \int_0^{x_m} F(x) x^{(p-2)/2} dx, \quad (5)$$

and denote the flux and the optical depth at a reference frequency $\nu_0 = 1$ GHz by f_0 and τ_0 respectively. The flux at other frequencies can then be obtained from

$$\frac{f_\nu}{f_0} = \frac{F_1(\nu)}{F_1(\nu_0)} \frac{F_2(\nu_0)}{F_2(\nu)} \left(\frac{\nu}{\nu_0} \right)^{5/2} \left\{ 1 - \exp \left[-\tau_0 \left(\frac{\nu_0}{\nu} \right)^{2+p/2} \frac{F_2(\nu)}{F_2(\nu_0)} \right] \right\}, \quad (6)$$

where the dependence of F_1 and F_2 on ν_m and p is suppressed for clarity. Note that the relative flux f_ν/f_0 depends on three parameters: τ_0 (the optical depth at $\nu_0 = 1$ GHz), ν_m (the characteristic frequency corresponding to the lowest electron energy) and p (the electron energy distribution index). By fitting the shape of radio spectrum at each day, we hope to determine these three parameters as a function of time.

The shape of the observed spectrum is specified by three spectral indices, between 20 cm/13 cm, 13 cm/6 cm, and 6 cm/3 cm (Fig. 2). In principle, one can invert equation (6) to determine the parameters τ_0 , ν_m and p uniquely from the three spectral indices. In practice, we adopt simple power-law distributions for these parameters as a function of time and compute and match the three spectral indices to the observed values as closely as possible. Through trial and error, we find that reasonable fits are obtained for

$$\tau_0 = 25 \left(\frac{t}{10 \text{ days}} \right)^{-2}; \quad \nu_m = 5.6 \left(\frac{t}{10 \text{ days}} \right)^{-1} \text{GHz}; \quad p = 2.5. \quad (7)$$

The fits are shown in Figure 2. We should point out that the spectral indices between 6 cm and 3 cm on day 3 and day 4 are not reproduced by our fits, indicating that processes other than synchrotron self-absorption might be important at such early times or that the simple power law

evolution breaks down. In addition, both ν_m and the self-absorption turnover frequency have moved below the observed frequency range by day 50 so these parameters are not constrained by the observations at later times. Over the time period that they are important for the observed radio emission, ν_m and the self-absorption turnover frequency are close to each other.

To convert the fitted optical depth τ_0 , characteristic frequency ν_m , and index p into physical quantities of the synchrotron emitting gas, we need to have a specific model for its geometry. Here we adopt the simplest model of a thin, uniform, spherical shell of radius r and thickness ξ (< 1) times the radius. For a given value of p , the optical depth, the frequency ν_m and the observed flux at a given frequency (say, 6 cm), we determine three physical quantities, which we choose to be the total energy E_i , the radius r and the electron density n_e .

For a power-law distribution of electrons given by equation (2), we have from the standard theory

$$\tau = \frac{p+2}{8\pi m\nu^2} \frac{\sqrt{3}q^3}{2mc^2} \left(\frac{4\pi mc\nu}{3q} \right)^{-p/2} F_2(\nu) C B_{\perp}^{(p+2)/2}(\xi r), \quad (8)$$

$$\nu_m = \frac{3\gamma_m^2 q B_{\perp}}{4\pi mc}, \quad (9)$$

$$f_{\nu} = \frac{\pi r^2}{d^2} \frac{2m\nu^2}{p+2} \left(\frac{4\pi mc\nu}{3qB_{\perp}} \right)^{1/2} \frac{F_1(\nu)}{F_2(\nu)} (1 - e^{-\tau}), \quad (10)$$

where the electron distribution coefficient C is related to the electron energy density U_e by

$$C = (p-2) \frac{U_e}{mc^2} \gamma_m^{p-2}, \quad (11)$$

and the minimum Lorentz factor γ_m is given, from equation (9), by

$$\gamma_m = \left(\frac{4\pi mc\nu_m}{3qB_{\perp}} \right)^{1/2}. \quad (12)$$

Making the usual assumption that the energy densities of electrons and magnetic fields are proportional to the total energy density U_i , we have $U_e = \epsilon_e U_i$ and $B_{\perp} = (8\pi\epsilon_b U_i)^{1/2}$. It turns out only two physical quantities enter equations (8) and (10) for the optical depth and the flux. They are the radius r of the emitting region and the total energy density U_i , or alternatively the total energy $E_i = 4\pi\xi r^3 U_i$. Straightforward but tedious algebraic manipulations show that

$$\begin{aligned} E_i = 1.26 \times 10^{49} & \left(\frac{0.1}{\epsilon_b} \right)^{6/17} \left(\frac{0.1}{\epsilon_e} \right)^{11/17} \left(\frac{\xi}{0.1} \right)^{6/17} \left(\frac{d}{40 \text{ Mpc}} \right)^{40/17} \\ & \left(\frac{f_{\nu}}{20 \text{ mJy}} \right)^{20/17} \left(\frac{p+2}{5} \right)^{9/17} \left(\frac{1}{p-2} \right)^{11/17} \left(\frac{\nu}{1 \text{ GHz}} \right)^{(11p-56)/34} \\ & \left(\frac{\nu_m}{1 \text{ GHz}} \right)^{11(2-p)/34} \frac{F_2(\nu)^{9/17} \tau^{11/17}}{F_1(\nu)^{20/17} (1 - e^{-\tau})^{20/17}} \text{ erg} \end{aligned} \quad (13)$$

and

$$\begin{aligned}
 r = 2.02 \times 10^{17} & \left(\frac{\epsilon_b}{0.1} \right)^{1/17} \left(\frac{0.1}{\epsilon_e} \right)^{1/17} \left(\frac{0.1}{\xi} \right)^{1/17} \left(\frac{d}{40 \text{ Mpc}} \right)^{16/17} \\
 & \left(\frac{f_\nu}{20 \text{ mJy}} \right)^{8/17} \left(\frac{p+2}{5} \right)^{7/17} \left(\frac{1}{p-2} \right)^{1/17} \left(\frac{\nu}{1 \text{ GHz}} \right)^{(p-36)/34} \\
 & \left(\frac{\nu_m}{1 \text{ GHz}} \right)^{(2-p)/34} \frac{F_2(\nu)^{7/17} \tau^{1/17}}{F_1(\nu)^{8/17} (1 - e^{-\tau})^{8/17}} \text{ cm.}
 \end{aligned} \quad (14)$$

In these expressions, the quantities p , ν_m and τ (as well as $F_1(\nu)$ and $F_2(\nu)$ implicitly) are given by equations (7) and (4), obtained from fitting the spectral shape of the radio emission. The flux f_ν is given by the observed radio light curves. We choose the smoothest curve of 6 cm, and fit it with an analytical expression, as shown in Figure 1. Other model curves on the same figure are obtained using the fitted parameters in equation (7). They match the data reasonably well. The weak dependence of r on ϵ_b/ϵ_e is comparable to that found for normal radio supernovae (Chevalier 1998).

From the fitted flux at 6 cm and equations (13)-(14), we obtain the time evolution of the total internal energy and the radius of synchrotron emitting gas. For a typical set of parameters $\epsilon_b = \epsilon_e = \xi = 0.1$ and $d = 40$ Mpc, we find a total energy between about $10^{49} - 3 \times 10^{49}$ erg and a radius between about $0.5 \times 10^{17} - 2.5 \times 10^{17}$ cm in the time interval from day 12 to day 80, as shown in panels (a)-(b) of Figure 4. For comparison, a straight line with a slope equal to the speed of light is drawn in panel (b), where the radius is plotted as a function of time. The average speed in this time interval is close to the speed of light, although the instantaneous value could be somewhat different.

We can also infer the number density of the emitting electrons, n_e . From equation (2), we have

$$n_e = \int_{\gamma_m}^{\infty} n(\gamma) d\gamma = \frac{p-2}{p-1} \frac{\epsilon_e}{mc^2} \frac{U_i}{\gamma_m}. \quad (15)$$

A straightforward substitution yields

$$\begin{aligned}
 n_e = 2.29 & \left(\frac{0.1}{\epsilon_b} \right)^{7/17} \left(\frac{\epsilon_e}{0.1} \right)^{7/17} \left(\frac{0.1}{\xi} \right)^{10/17} \left(\frac{40 \text{ Mpc}}{d} \right)^{10/17} \\
 & \left(\frac{20 \text{ mJy}}{F_\nu} \right)^{5/17} \left(\frac{5}{p+2} \right)^{15/17} \frac{(p-2)^{7/17}}{p-1} \left(\frac{\nu}{1 \text{ GHz}} \right)^{(10p+65)/34} \\
 & \left(\frac{\nu_m}{1 \text{ GHz}} \right)^{(3-10p)/34} \frac{F_1(\nu)^{5/17} \tau^{10/17} (1 - e^{-\tau})^{5/17}}{F_2(\nu)^{15/17}} \text{ cm}^{-3}.
 \end{aligned} \quad (16)$$

This quantity is shown as a function of radius in panel (c) of Figure 4. Clearly, the number density of the emitting electrons drops off with radius approximately as r^{-2} . Since the density in the emitting region is related to the density in the ambient medium (which supplies the emitting gas with matter through a strong shock) by a simple compression factor, we conclude that the

ambient medium must have a r^{-2} density profile as well. Such a profile arises naturally in a stellar wind of constant mass loss rate and constant velocity from the progenitor star of the supernova. We can estimate the mass loss rate in the wind through

$$\dot{M}_w = 4\pi\rho_w V_w r^2 = 4.67\pi\xi n_e m_p r^2 V_w, \quad (17)$$

where the subscript “ w ” stands for the wind and a fully ionized postshock medium with 10% of helium by number is assumed. We plot the inferred mass flux as a function of radius in panel (d) of Figure 4. For the typical parameters chosen, we have a stellar mass loss rate of order $3 \times 10^{-7} (V_w/10^3 \text{ km s}^{-1}) M_\odot \text{ yr}^{-1}$. The dependence on the parameters ϵ_b and ϵ_e can be found from equation (16).

4. DYNAMICAL AND RELATIVISTIC EFFECTS

So far, we have worked directly with the radio data and inferred from it properties of the emitting region using a simple radiation model. Now we use these results as a guide and construct a more detailed model taking into account the dynamics of the emitting matter and relativity - two principal effects neglected in the above approach.

We envision an instantaneous release of a large amount of energy E_0 in a r^{-2} -density external medium. The energy released drives in the medium a blast wave, whose dynamics can be deduced approximately from the following considerations. In the frame at rest with respect to the origin of the explosion (and the observer), let the shocked external material be distributed uniformly in a shell of thickness ΔR_s (much less than the outer radius of the shell, the shock radius R_s). The physical quantities inside the shell are related to those of the external medium by a set of shock-jump conditions. For a strong shock of ultrarelativistic speed, the conditions are given by Blandford & McKee (1976). Slight modifications are needed for our application, where the shock speed is likely transrelativistic. Let γ be the bulk Lorentz factor of the shocked medium in the shell and Γ that of the shock front. The modified jump conditions are

$$e' = \frac{\eta\gamma + 1}{\eta - 1}(\gamma - 1)n m_p c^2, \quad (18)$$

$$n' = \frac{\eta\gamma + 1}{\eta - 1}n, \quad (19)$$

where e' and n' are the energy and number densities of the shell in its comoving frame, and η is the adiabatic index, which equals 4/3 for ultrarelativistic shocks and 5/3 for nonrelativistic shocks. A simple interpolation between these two limits,

$$\eta = \frac{4\gamma + 1}{3\gamma}, \quad (20)$$

should be valid approximately for transrelativistic shocks as well (Huang, Dai & Lu 1998). The symbol m_p denotes the mass of protons while n is the number density of the external medium

(assumed in this section to be purely hydrogenic for simplicity),

$$n = \frac{n_0 r_0^2}{r^2}, \quad (21)$$

where n_0 and r_0 are constants. The Lorentz factor of the shock front is given by

$$\Gamma^2 = \frac{(\gamma + 1)[(\eta(\gamma - 1) + 1)^2]}{\eta(2 - \eta)(\gamma - 1) + 2}, \quad (22)$$

which depends on the shell Lorentz factor γ .

The shell Lorentz factor γ is determined by the conservation of mass

$$4\pi R_s^2 \Delta R_s \hat{n} = 4\pi n_0 r_0^2 R_s \quad (23)$$

and the conservation of energy

$$4\pi R_s^2 \Delta R_s \hat{e} = E_0, \quad (24)$$

where the energy density \hat{e} and the number density \hat{n} of the shell in the frame at rest with respect to the origin are related to those in the comoving frame by the transformation

$$\hat{e} = \frac{4\gamma^2 - 1}{3} e', \quad \hat{n} = \gamma n'. \quad (25)$$

Combining equations (23)-(25) we obtain an algebraic equation for γ

$$\frac{(\gamma - 1)(4\gamma^2 - 1)}{3\gamma} = \frac{E_0}{4\pi m_p c^2 n_0 r_0^2 R_s} \quad (26)$$

in terms of the shock radius R_s . The shock radius itself evolves according to

$$\frac{dR_s}{dt} = c\sqrt{1 - \Gamma^{-2}}, \quad (27)$$

where t is the time since explosion in the rest frame of the origin. This completes our discussion of the blast wave dynamics.

To properly calculate emission from transrelativistic blast waves, one needs to take into account the finite light-travel time (Rees 1967). To facilitate discussion, let us adopt a cylindrical coordinate system (R, ϕ, z) , with the z -axis pointing from the origin of the blast wave toward the observer (see Figure 5). Let T be the time in the observer's frame. A light pulse emitted at a time t in the rest frame of the origin from a location at an axial distance z is received by the observer at a time

$$T = t - z/c. \quad (28)$$

Our goal is to calculate the specific intensity I_ν on the surface of the shell facing the observer at a distance R from the axis at an observer's time T , $I_\nu(T, R)$. It depends on the emission and absorption coefficients at different values of z , $j_\nu(T, R, z)$ and $\kappa_\nu(T, R, z)$. We need to determine

which part of the shell contributes to the emission and absorption at (T, R, z) . In what follows, we describe a mathematical procedure for such a determination.

At any given time t , the inner and outer radii of the emitting shell are known from the blast wave dynamics. It is easy to calculate the time T for radiation emitted at a distance R from the axis to arrive at the observer from equation (28). The possible arrival time fills a band of “V” shape on the $T - t$ diagram for a given distance R , as shown in Figure 6. Its shape depends on the thickness and dynamics of the shell as well as the off-axis distance R . One can read off this $T - t$ diagram the time t when the emission from the shell at an off-axis distance R can reach the observer at any given time T . Once the time t is determined, the axial distance of the emitting region is given by

$$z = c(t - T). \quad (29)$$

From equations (18) and (19), we can determine the comoving energy and number densities, e' and n' . It is then a simple matter to calculate the emission and absorption coefficients, $j'_{\nu'}(T, R, z)$ and $\kappa'_{\nu'}(T, R, z)$, in the comoving frame as a function of the comoving frequency ν' . To obtain radiation quantities in the rest frame of the origin, we use the following standard transformation (e.g., Rybicki & Lightman 1979):

$$\nu = \frac{\nu'}{\gamma(1 - \beta\mu)}, \quad (30)$$

$$j_{\nu}(T, R, z) = \frac{j'_{\nu'}(T, R, z)}{[\gamma(1 - \beta\mu)]^2}, \quad (31)$$

$$\kappa_{\nu}(T, R, z) = \kappa'_{\nu'}[\gamma(1 - \beta\mu)], \quad (32)$$

where γ and $\beta = (1 - \gamma^{-2})^{1/2}$ are the Lorentz factor and the speed (in units of c) of the emitting shell material, and

$$\mu = \frac{z}{\sqrt{R^2 + z^2}} \quad (33)$$

is the cosine of the angle between the symmetry axis and the line passing through the origin and the emitting point.

With the emission and absorption coefficients j_{ν} and κ_{ν} determined as a function of axial distance z , one can write down the radiative transfer equation along lines parallel to the axis

$$\frac{dI_{\nu}(T, R, z)}{dz} = j_{\nu}(T, R, z) - \kappa_{\nu}(T, R, z)I_{\nu}(T, R, z). \quad (34)$$

With the usual definition of optical depth $d\tau_{\nu} = -\kappa_{\nu}dz$ we find that the specific intensity at the surface facing the observer (where $\tau_{\nu} = 0$) is given by

$$I_{\nu}(T, R, \tau_{\nu} = 0) = \int_0^{\tau_{max,\nu}} S_{\nu}(T, R, \tau_{\nu})e^{-\tau_{\nu}}d\tau_{\nu} \quad (35)$$

where

$$\tau_{max,\nu} = \int_{-\infty}^{\infty} \kappa_{\nu}dz \quad (36)$$

is the total optical depth through the shell at an off-axis distance of R while

$$S_\nu = \frac{j_\nu}{\kappa_\nu} \quad (37)$$

is the source function. Finally, we integrate over the surface of the shell to obtain the total flux at the time T and the frequency ν

$$F_\nu(T) = \frac{2\pi}{d^2} \int_0^{R_{max}} I_\nu(T, R, \tau_\nu = 0) R dR. \quad (38)$$

With this formalism, we explore numerically various combinations of parameters, trying to determine the best fits to the observed radio light curves.

Our procedure was to choose ϵ_b and ϵ_e and then to vary the energy and ambient density until the best fit to the data was obtained. For the same magnetic and electron energy factors $\epsilon_b = \epsilon_e = 0.1$, power index of electron energy distribution $p = 2.5$, and source distance $d = 40$ Mpc as in the last section, we find that a total energy of $E_0 = 1.5 \times 10^{49}$ erg and a value of $n_0 r_0^2 = 1.14 \times 10^{34}$ cm $^{-1}$ for the external r^{-2} -density medium fit the radio light curves before the second bumps (around day 24) reasonably well (see Figure 7). The value for the external medium corresponds to a stellar wind mass loss rate of $3.8 \times 10^{-7} (V_w/10^3 \text{ km s}^{-1}) M_\odot \text{ yr}^{-1}$. Therefore, both the total explosion energy and the wind mass loss rate are not far from those inferred in the last section. In other words, the corrections due to dynamical and relativistic effects are relatively modest: they are of factors of two or less.

After about day 24, the observed fluxes increase dramatically at all four frequencies. These increases are incompatible with the predictions of a simple constant-energy blast wave model, as evident in Figure 7. The predicted fluxes are too small by a factor of two to three at later times. A resolution of this discrepancy is suggested by Figure 4(a), where a sudden increase of energy supply is implied. We therefore consider the simplest case where the total energy of the blast wave increases from its initial value of E_0 to a final value of E_1 instantaneously at a time t_1 (in the rest frame of the origin). After some experimentation, we find that the combination of $E_1 = 4.2 \times 10^{49}$ erg and $t_1 = 105$ days fits the late time light curves reasonably well (Figure 7). The fitting is not perfect, nor is it expected to be, given the idealized nature of our model. In calculating the blast wave dynamics and the radio emission, we have assumed that the promptly injected energy is shared instantaneously by all material in the uniform shell, which leads to a jump in the velocity and other properties of the emitting shell (see Figure 8). The transrelativistic nature of the emitting region is clear in Figure 8, with a speed $\beta = v/c$ between 0.6 to about 0.9 in the time interval of interest. It is interesting to note that the energy injection occurs about 100 days after the explosion. Relativistic effects make its presence felt much earlier in the light curves in the observer's frame, around day 22. Also, the jump in energy is substantial, by a factor of ~ 2.8 .

The inferred total energy and dynamics of the blast wave depend on the magnetic and electron energy factors. To illustrate the dependence, we consider the extreme case with a tiny magnetic

energy factor $\epsilon_b = 10^{-6}$ and a maximum possible electron energy factor $\epsilon_e = 1$ ¹. These parameters are close to those used by Waxman & Loeb (1999) in their subrelativistic model for RSN 1998bw with a thermal electron distribution. For a power index of electron energy distribution $p = 2.5$ and source distance $d = 40$ Mpc as before, we find a reasonable fit to the observed radio emission (see Figure 9) for the following set of parameters: a total initial energy of $E_0 = 2.1 \times 10^{50}$ erg; a stellar wind mass loss rate of $7.2 \times 10^{-5} (V_w/10^3 \text{ km s}^{-1}) M_\odot \text{ yr}^{-1}$; and a jump to a total energy of $E_1 = 5.5 \times 10^{50}$ erg at a time $t_1 = 50$ days in the rest frame of the origin. Note that the rising parts of all four model light curves at days 20 – 40 are nearly parallel to one another, in a better agreement with observations than the case with $\epsilon_b = \epsilon_e = 0.1$ considered earlier (see Figure 7). The reason is that the shock speed, also shown in Figure 8, is significantly lower in the $\epsilon_b = 10^{-6}$ case than in the $\epsilon_b = 0.1$ case in the time interval of interest; a lower shock speed tends to steepen the rise in the radio fluxes at short, optically thin wavelengths, since a larger portion of the re-energized shell contributes to the total emission at the given time. Compared to the model of Waxman & Loeb (1999), which was primarily intended for the observations on day 12, our model has a higher shock velocity ($0.6c$ vs. $0.3c$) and a higher energy by a factor of a few. The differences may be related to the fact that our model has a decelerating shock wave, includes relativistic effects, and assumes a power law electron distribution.

These models show that models with a wide range of ϵ_b can approximately represent the data. The scaling between these models is discussed in the next section. However, we have found that acceptable models are even more widely distributed and can be found with $\epsilon_e = 0.01$. It appears that changes in ν_m and changes in the time lag effects can cancel each other out. The energy and ambient density of these models remains in the range of those given above.

We have also investigated models in which the flux rise is due to a jump in the ambient density instead of an energy increase. Although it is possible to obtain an increase in the extrapolated flux going to late times, it is not possible to obtain a fit during the transition period (20-40 days). In particular, the fluxes remain flat during this period instead of rising.

5. POWER LAW DYNAMICS

Many of the previous discussions of GRB afterglow light curves have assumed power law evolution based on smooth properties of the ejecta and the surrounding medium (Mészáros, Rees, & Wijers 1998 and references therein). RSN 1998bw shows a more complex evolution, but our model indicates that over substantial periods of time the evolution is described by a constant energy shell in a $\rho \propto r^{-2}$ medium. During these times the radio flux evolution is described by $F_\nu \propto t^{-1.6}$ at optically thin wavelengths. Mészáros, Rees, & Wijers (1998) discuss the expected

¹Strictly speaking, the choice $\epsilon_e = 1$ is not consistent with our blast wave model which assumes implicitly that most of the energy is carried by protons. It should be adequate for a rough parameter study, however.

power law evolution in a $\rho \propto r^{-2}$ medium for a relativistic flow and find that for $\nu > \nu_m$ and constant energy, $F_\nu \propto t^{(1-3p)/4}$. For $p = 2.5$, we have $F_\nu \propto t^{-1.62}$, in good agreement with the observations of RSN 1998bw. The observed time period 12–24 days is especially useful because self-absorption and ν_m affect the evolution and provide diagnostic information. The optical depth at 1.4 GHz is moderately high and we expect $F_\nu \propto r^2 \propto t$, which is in agreement with the observations (Fig. 1).

The fact that a constant energy explosion in a $\rho \propto r^{-2}$ medium describes the $t = 12 - 24$ day evolution can be used to find scaling relations for the acceptable models. The model parameters are E , A (where $\rho = Ar^{-2}$), ϵ_e , and ϵ_b . The parameter p is simply determined by the observations. The observational constraints on these parameters can be described by ν_m , F_{ν_m} , and ν_A , where ν_A is the frequency at which the spectrum becomes self-absorbed. The expected evolution of these quantities for a relativistic explosion in an r^{-2} medium is (cf. Waxman 1997; Mészáros et al. 1998)

$$\nu_m \propto \epsilon_e^2 \epsilon_b^{1/2} E^{1/2} t^{-3/2}, \quad (39)$$

$$F_{\nu_m} \propto \epsilon_b^{1/2} A E^{1/2} t^{-1/2}, \quad (40)$$

$$\nu_A \propto \epsilon_e^{-1} \epsilon_b^{1/5} A^{6/5} E^{-2/5} t^{-3/5}. \quad (41)$$

There are 3 constraints on the 4 model parameters, so there is not expected to be a unique model fit to the data. One way of describing the scaling of acceptable models is to fix ν_m , F_{ν_m} , and ν_A at some time t and find how 3 of the model parameters depend on the fourth one. For example, we find

$$E \propto \epsilon_b^{-1/5}, \quad A \propto \epsilon_b^{-2/5}, \quad \epsilon_e \propto \epsilon_b^{-1/5}. \quad (42)$$

If one dynamical model with $\epsilon_b = 0.1$ and $\epsilon_e = 0.1$ fits the data, then another model with $\epsilon_b = 10^{-6}$, $\epsilon_e \sim 1$, E up by 10, and A up by 100 should fit the data equally well. This is in approximate accord with the results in the previous section. In the opposite direction, increasing ϵ_b to equipartition with the postshock gas ($\epsilon_b = 0.5$) leads to moderately small decreases in the other parameters. Our detailed models, discussed in the previous section, show that the range of acceptable parameters is broader. The emission is not from a single region, as is assumed in the power law model, but is integrated over a shell with time lags. These conditions allow a greater variety of models.

For the flux evolution in the optically thin regime, equations (39) and (40) can be combined to yield

$$F_\nu \propto \epsilon_e^{p-1} \epsilon_b^{(p+1)/4} A E^{(p+1)/4} t^{(1-3p)/4}. \quad (43)$$

The observed flux increase from before day 24 to after day 32 is a factor of 2.2 (see § 2). If this increase is due to an energy increase, equation (43) shows that $E \propto F_\nu^{4/(p+1)}$ and so E must increase by a factor of 2.5 for $p = 2.5$. This result is in approximate agreement with the factor of 2.6–2.8 found in the detailed models. The failure of a density increase to account for the flux rise can also be seen from the power law dynamics. The flux at an optically thick wavelength

is expected to increase as r^2 . A boost in the shock energy accelerates the expansion rate and accelerates the flux increase. An increase in the ambient density decelerates the shock and the flux increase. The data at 1.4 GHz, an optically thick wavelength, show an accelerating rise through the time of the flux increase. The implication is that the increase is due to an energy, not a surrounding density, increase, which is in accord with our detailed models.

An extrapolation of the constant E evolution to day 10 and earlier yields fluxes at 8.6 GHz that are higher than those observed. Equation (41) shows that an attempt to model this solely as an energy jump yields a higher value of ν_A at early times. This would imply that the observed spectrum should be in the self-absorbed regime, or $F_\nu \propto \nu^2$. The observed spectrum is not compatible with this form, which shows that the early flux increase cannot be explained in the same way as the later one.

6. RSN 1998bw AND GRB 980425

Our models have implications for the nature of RSN 1998bw in the context of SN 1998bw and the possibly associated GRB 980425. Models for the light curve and some spectra of SN 1998bw indicate that the progenitor star was the heavy element core of a massive star with a final mass of $13.8 M_\odot$ (Iwamoto et al. 1998) or $6 M_\odot$ (Woosley et al. 1999). Such stars are observed as Wolf-Rayet stars, which have winds with velocities in the $V_w = 1,000 - 2,500 \text{ km s}^{-1}$ range and mass loss rates $\dot{M} = 10^{-5} - 10^{-4} M_\odot \text{ yr}^{-1}$ (Willis 1991). Our $\epsilon_b = 0.1$ model for RSN 1998bw implies $\dot{M}/V_w \approx (4 \times 10^{-7} M_\odot \text{ yr}^{-1})/(1,000 \text{ km s}^{-1})$ and the $\epsilon_b = 10^{-6}$ model implies $\dot{M}/V_w \approx (7 \times 10^{-5} M_\odot \text{ yr}^{-1})/(1,000 \text{ km s}^{-1})$. The density range in the models overlaps the circumstellar density expected for a Wolf-Rayet star; the high ϵ_b models yield a density that is somewhat too low, so there is a preference for the low ϵ_b models. The low ϵ_b models also appear to fit the rise in the radio light curves at days 20 – 40 better.

The blast wave energies estimated during the observed period beginning on day 12 range from 1.5×10^{49} ergs with $\beta = v/c \gtrsim 0.8$ for the $\epsilon_b = 0.1$ model and 2×10^{50} ergs with $\beta \gtrsim 0.5$ for the $\epsilon_b = 10^{-6}$ model. Immediately after the impulsive energy increase, the energies are 4×10^{49} ergs and 5×10^{50} ergs with $\beta \approx 0.85$ and $\beta \approx 0.6$ for the high and low ϵ_b models, respectively. These energies can be compared to those expected in the shock-accelerated high velocity ejecta of SN 1998bw. There is the possibility that the high radio luminosity is simply because of the higher explosion energy than that normally found in Type Ib/c supernovae. Woosley et al. (1999) estimate that their model for SN 1998bw produces 5×10^{49} ergs of ejecta with $\beta = c/3$. Although their models are nonrelativistic, Matzner & McKee (1999) estimate the relativistic mass ejection that can be expected from an explosion like SN 1998bw. They note that a stripped massive star may not be sufficiently compact to produce any relativistic ejecta. A 3×10^{52} erg explosion with $6 M_\odot$ of ejecta in a sufficiently compact star should yield $\sim (1-2) \times 10^{48}$ ergs of relativistic ejecta. The shock acceleration process yields a mass (and energy) that declines steeply with velocity, so the results are sensitive to the details of the model. The energy inferred for RSN 1998bw appears

to be too high for the shock accelerated ejecta of SN 1998bw, but this result is not conclusive.

Our model also places constraints on the time dependence of the energy input to the blast wave. For $t > 12$ days, we find that the blast wave evolves with approximate constant energy except for an episode during which the energy is increased by a factor ~ 3 . The change does not appear to be due to the circumstellar medium and is probably due to inner material that catches up with the interaction region. This type of evolution is not expected for energy injection from shock-accelerated, high velocity supernova ejecta, which presumably have a smooth distribution. This property, along with the high energy in RSN 1998bw, suggests the presence of a central engine in the explosion. The fact that RSN 1998bw was accompanied by a Type Ic supernova with $\sim 10 M_{\odot}$ of material moving at moderate velocity (Galama et al. 1998b; Iwamoto et al. 1998), implies that the high velocity outflow giving rise to RSN 1998bw is not spherically symmetric, but occupies only a fraction of the total 4π solid angle. MacFadyen & Woosley (1999) have proposed a model for SN 1998bw in which beamed, high-energy flows are created by a disk around a central black hole. The success of spherically symmetric models in describing normal GRBs is usually attributed to relativistic beaming; only a small part of a possibly asymmetric source is being observed. This argument does not apply to our model for RSN 1998bw because the velocities are only mildly relativistic and it is thus surprising that a spherically symmetric model is so successful. The introduction of asymmetries in the models brings in new parameters and we have not investigated such models.

The type of evolution that is observed in RSN 1998bw may be related to that observed in the optical afterglow of GRB 970508. In that case, there is evidence for a steady or decreasing flux before the 1.5 day rise phase leading to the maximum (Pedersen et al. 1998). An extrapolation of the early evolution implies that the rise is by a factor of 4. Mésza  s, Rees, & Wijers (1998) suggest that the rise is due to a multicomponent flow or to a lower Γ shell catching up with the main shock front. Both of these models have been calculated in more detail by Panaiteescu, M  sza  s, and Rees (1998). In their model with late impulsive energy input, the energy increases from 0.6×10^{52} ergs to 2.4×10^{52} ergs. Although the energies are larger than those inferred in RSN 1998bw, the factor increase in energy is comparable to the one that we have advocated for RSN 1998bw. A multicomponent flow model does not appear plausible for RSN 1998bw because of the continuity of the radio spectral indices during the time of the flux increase.

The fact that we have found that RSN 1998bw has a central engine related to those found in normal GRBs strengthens the association with GRB 980425 and suggests that the relation of the radio emission to the early γ -ray emission be investigated. However, there are several reasons why an energy conserving synchrotron model cannot be simply extrapolated back to the very early times (cf. Iwamoto 1999). First, we have found evidence in the radio light curves for at least one episode of impulsive energy injection. Additional episodes could have also occurred before day 3 when the radio observations were initiated. The result would be lower flux values at early times. Second, synchrotron losses become more important at early times. The frequency at which the synchrotron loss time equals the age is $\nu_c \propto t^{1/3}$ for constant energy evolution in an

r^{-2} medium. The peak frequency evolves as $\nu_m \propto t^{-3/2}$, so that the blast wave was radiative in the past. Taking $\nu_m = 5.6$ GHz on day 10 implies radiative evolution before $t \sim 1$ day. Third, the unusual behavior observed between days 3 and 12 may indicate that it may not be possible to extrapolate the $\rho \propto r^{-2}$ medium to small radii. Finally, the early evolution may be affected by the character of the initial injection of energy. If the shell has an initial Lorentz factor Γ_o , its mass is $M = E_o/\Gamma_o c^2$, where E_o is the initial energy. The deceleration radius, r_{dec} , occurs when the shell has swept up a mass $\Gamma_o M$ in the circumburst environment. Thus

$$r_{\text{dec}} = \frac{E_o}{\Gamma_o^2 c^2 (\dot{M}/V_w)} = 2 \times 10^{12} E_{o48} \Gamma_{o1}^{-2} \left(\frac{\dot{M}/V_w}{6.3 \times 10^{12} \text{ g cm}^{-1}} \right)^{-1} \text{ cm}, \quad (44)$$

where $E_{o48} = E_o/(10^{48} \text{ ergs})$, $\Gamma_{o1} = \Gamma_o/10$, and the reference value of \dot{M}/V_w corresponds to $\dot{M}/V_w = (1 \times 10^{-5} M_\odot \text{ yr}^{-1})/(1,000 \text{ km s}^{-1})$. The energy $E_o = 10^{48} \text{ ergs}$ is a lower limit based on the radiated energy in γ -rays. The shell radius at $t = 10$ s is $r \approx 2\Gamma_o^2 c t = 6 \times 10^{13} \Gamma_{o1}^2 \text{ cm}$. If Γ_o starts at the lower end of the plausible range or if E_o is high, the burst observations may be during the initial deceleration period. Other possible factors are electron scattering opacity and $\gamma - \gamma$ opacity for the GRB. If the electron scattering opacity is $0.4 \text{ cm}^2 \text{ g}^{-1}$, as expected for a baryon dominated plasma, electron scattering is not important. For the relatively low energy burst considered here, $\gamma - \gamma$ opacity is not important (cf. Piran 1996).

7. CONCLUSIONS

We have modeled the radio emission from SN 1998bw as the synchrotron emission from a rapidly expanding shock wave. We assumed that the electron energy and the magnetic energy densities are constant fractions of the postshock energy density, as is commonly done in models of both radio supernovae and GRB afterglows. The result of our modeling is that the radio evolution is consistent with expansion into a $\rho \propto r^{-2}$ circumstellar wind. The estimated wind density is consistent with that expected around the progenitor star that gave rise to the optical SN 1998bw and with the type of environment commonly deduced around radio supernovae. However, the radio light curves show two periods of flux increase that appear to require episodes of impulsive energy injection. The evolution between these times of injection are consistent with constant blast wave energy. We speculate that the freely expanding explosion ejecta contain shells that catch up with and energize the blast wave.

Katz (1999) has recently proposed a different model for RSN 1998bw in which the power for the source is provided by radioactivity. The γ -rays lines from radioactivity Compton scatter electrons which then move out in a mildly relativistic flow. Possible problems for the model are that the ^{56}Ni produced in the explosion must be mixed to the surface of the debris and the origin of the energetic electrons needed for the synchrotron emission is unclear.

The association of SN 1998bw with GRB 980425 appears likely based not only on the spatial and temporal coincidence of the events (Galama et al. 1998b), but also on the unusually

high energies of the optical and radio supernova phenomena. The finding that the ejecta are in discrete shells gives additional evidence for a relation between the two events because the ejecta in normal radio supernovae are inferred to be approximately smoothly distributed, as expected for shock-accelerated ejecta. The optical light curve of the GRB 970508 afterglow indicates discrete structure in the ejecta; in other GRB cases, the evolution can be described by a constant energy model as is also inferred for substantial parts of the evolution of RSN 1998bw. Although the environment of RSN 1998bw is similar to that inferred around normal radio supernovae, the explosion event shows a link to the more energetic GRBs. Woosley et al. (1999) and MacFadyen & Woosley (1999) have also linked SN 1998bw to the GRBs based on the high energy of the event. In the model of MacFadyen & Woosley (1999), energy for the outflow is provided by neutrino-antineutrino annihilations soon after the formation of a central black hole. Another possibility is the formation of a “microquasar” inside of a massive star (Paczyński 1998).

Cosmological GRBs with well-observed afterglows, including GRB 970228 (Wijers et al. 1997) and GRB 970508 (Waxman 1997; Granot, Piran, & Sari 1998), have been inferred to be expanding into a medium with a low, constant density ($n_o \approx 1 \text{ cm}^{-3}$). Power law declines are observed, but with a time dependence $F_\nu \propto t^{-w}$ with $w = 1.10 - 1.20$. The steeper decline observed in RSN 1998bw ($w = 1.6$) is an important part of the evidence for expansion in a $\rho \propto r^{-2}$ medium. The steeper decline is also expected for the optical and X-ray afterglows, which can account for the unusual lack of an X-ray afterglow if SN 1998bw is associated with GRB 980425. The expected early radiative losses are another factor (Bloom et al. 1998).

Bloom et al. (1998) have discussed the notion that the SN 1998bw/GRB 980425 event is a prototype of a new class of GRB associated with supernovae (S-GRB). One of the attractive features of the association was that the single pulse nature of GRB 980425 could be attributed to the shock wave generated by the smooth, shock-accelerated ejecta, which are not expected to contain internal shocks. In our model, the radio emission is driven by ejecta with considerable structure so that the association with a single pulse GRB may not be significant. However, our work has brought out another suggestive distinction between the S-GRB and normal GRBs. RSN 1998bw shows evidence for interaction with a circumstellar wind, as expected for its massive star progenitor. In the cases where there are sufficient data to make a determination, the observations of normal GRBs are consistent with interaction with a medium with a low, constant density. The situation is not expected in the immediate vicinity of a massive star and may point to a different kind of progenitor object in these cases.

We are grateful to Dale Frail and Shri Kulkarni for information on their radio observations. Support for this work was provided in part by NASA grant NAG5-8232.

REFERENCES

Ball, L., Campbell-Wilson, D., Crawford, D. F., & Turtle, A. J. 1995, *ApJ*, 453, 864

Blandford, R. D., & McKee, C. F. 1976, *Phys. Fluids*, 19, 1130

Bloom, J. S., Kulkarni, S. R., Harrison, F., Prince, T., Phinney, E. S., & Frail, D. A. 1998, *ApJ*, 506, L105

Chevalier, R. A. 1982, *ApJ*, 259, 302

Chevalier, R. A. 1998, *ApJ*, 499, 810

Fransson, C., & Björnsson, C.-I. 1998, *ApJ*, 509, 861

Galama, T. J., Wijers, R. A. M. J., Bremer, M., Groot, P. J., Strom, R. G., Kouveliotou, C., & van Paradijs, J. 1998a, *ApJ*, 500, L97

Galama, T. J., et al. 1998b, *Nature*, 395, 670

Granot, J., Piran, T., & Sari, R. 1998, *ApJ*, submitted (astro-ph/9808007)

Huang, Y. F., Dai, Z. G., & Lu, T. 1998, *A&A*, 336, L69

Iwamoto, K. 1999, *ApJ*, 512, L47

Iwamoto, K., et al. 1998, *Nature*, 395, 672

Katz, J. I. 1999, preprint

Kulkarni, S. R., Frail, D. A., Wieringa, M. H., Ekers, R. D., Sadler, E. M., Wark, R. M., Higdon, J. L., Phinney, E. S., & Bloom, J. S. 1998, *Nature*, 395, 663

MacFadyen, A., & Woosley, S. E. 1999, *ApJ*, in press (astro-ph/9810274)

Matzner, C. D., & McKee, C. F. 1999, *ApJ*, 510, 379

Mészáros, P., Rees, M. J., & Wijers, R. A. M. J. 1998, *ApJ*, 499, 301

Paczynski, B. 1998, *ApJ*, 494, L45

Panaitescu, A., Mészáros, P., & Rees, M. J. 1998, *ApJ*, 503, 315

Pedersen, H., et al. 1998, *ApJ*, 496, 311

Pian, E. et al. 1999, *A&A*, in press (astro-ph/9903113)

Piran, T. 1996, in *Unsolved Problems in Astrophysics*, ed. J. N. Bahcall & J. P. Ostriker (Princeton: PUP), 343

Rees, M. J. 1967, MNRAS, 135, 345

Rybicki, G. B., & Lightman, A. P. 1979, Radiative Processes in Astrophysics (New York: Wiley)

Slysh, V. I. 1990, Sov. Astr. Lett., 16, 339

Van Dyk, S. D., Weiler, K. W., Panagia, N., & Sramek, R. A. 1994a, in Circumstellar Media in the Late Stages of Stellar Evolution, ed. R. E. S. Clegg, I. R. Stevens, & W. P. S. Meikle (Cambridge: CUP), 112

Van Dyk, S. D., Weiler, K. W., Sramek, R. A., Rupen, M. P., & Panagia, N. 1994b, ApJ, 432, L115

Waxman, E. 1997, ApJ, 489, L33

Waxman, E., & Loeb, A. 1999, ApJ, in press (astro-ph/9808135)

Weiler, K. W., Montes, M. J., Van Dyk, S. D., Sramek, R. A., & Panagia, N. 1999, in SN 1987A: 10 Years Later, ed. M. Phillips & N. Suntzeff (San Francisco: ASP), in press

Weiler, K. W., Van Dyk, S. D., Panagia, N., & Sramek, R. A. 1992, ApJ, 398, 248

Weiler, K. W., Van Dyk, S. D., Montes, M. J., Panagia, N., & Sramek, R. A. 1998, ApJ, 500, 51

Wieringa, M. H., Kulkarni, S. R., & Frail, D. A. 1999, A&A, in press

Wijers, R. A. M. J., Rees, M. J., Mészáros, P. 1997, MNRAS, 288, L51

Willis, A. J. 1991, in Wolf-Rayet Stars and Interrelations with Other Massive Stars in Galaxies, ed. K. A. van der Hucht & B. Hidayat (Dordrecht: Kluwer), 265

Wink, J. E. H. 1994, IAUC, No. 6009

Woosley, S. E., Eastman, R. G., & Schmidt, B. P. 1999, ApJ, in press (astro-ph/9806299)

Fig. 1.— The full observed radio fluxes and the nonrelativistic model fits for day 12 and later. As explained in § 3, the flux at 6 cm is fitted analytically. Together with the model spectral indices shown in Figure 2, it yields the model fluxes at other wavelengths.

Fig. 2.— Spectral indices of radio emission at day 12 and later. The solid lines are model fits using a simple synchrotron self-absorption model with electrons in a power-law energy distribution truncated from below. The fitted quantities are shown in equation (7).

Fig. 3.— The peak spectral luminosity vs the product of the time of the peak and the frequency of the measurement, based on Fig. 4 of Chevalier (1998) with the addition of SN 1998bw. The observed supernovae are designated by the last two digits of the year and the letter, and are of Types II (*stars*), Ib (*squares*), and Ic (*crosses*). The dashed lines show the mean velocity of the radio shell if synchrotron self-absorption is responsible for the flux peak; a value $p = 2.5$ is assumed.

Fig. 4.— Deduced quantities of a uniform, nonrelativistically moving shell between day 12 and day 80 from model fits to the observed spectral indices and the 6 cm flux. Shown are (a) the time evolution of the total energy, (b) the evolution of the shock radius, (c) the electron density in the emitting shell as a function of radius, and (d) the ratio of the mass loss rate and speed of the progenitor’s wind.

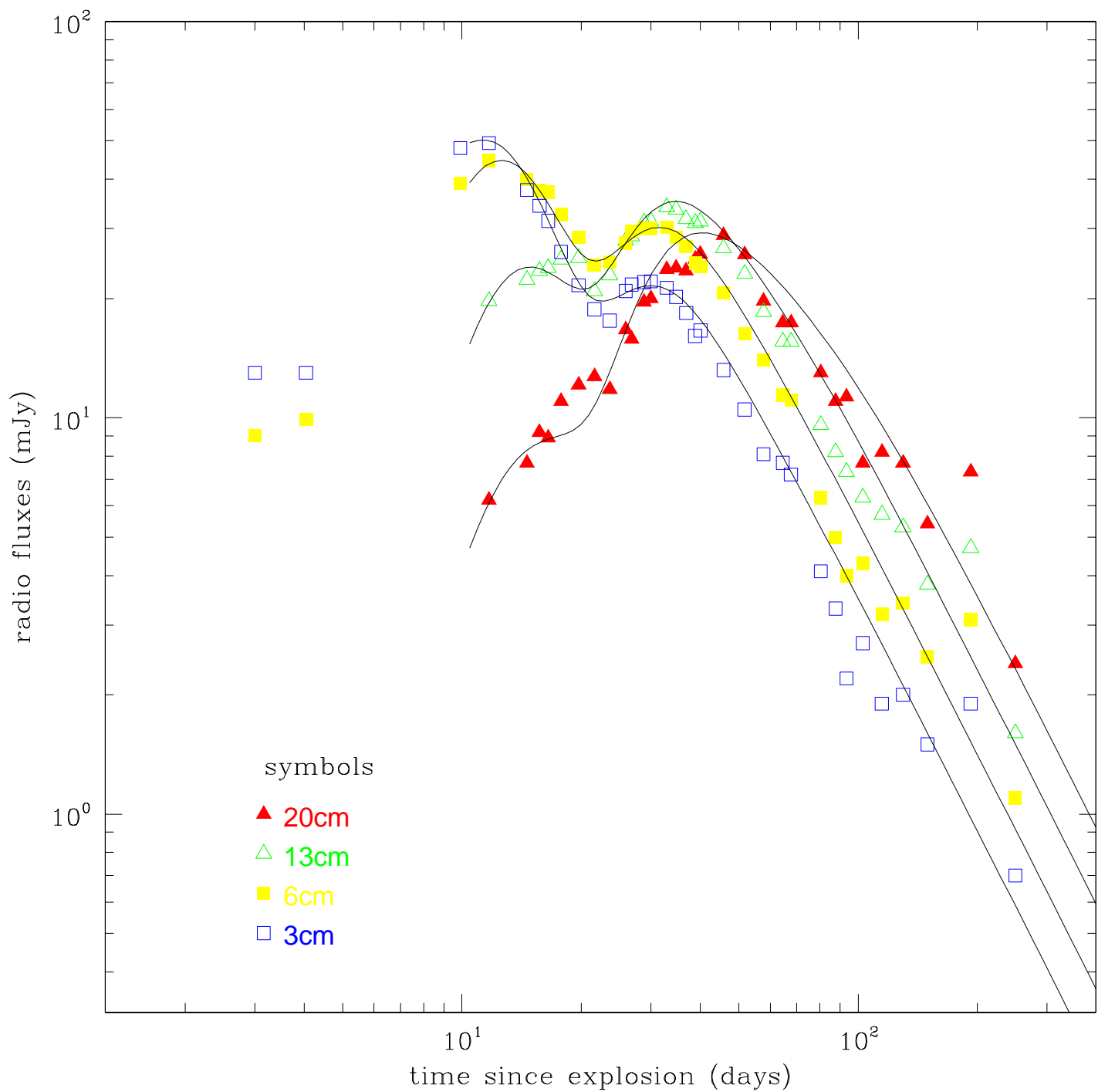
Fig. 5.— The coordinate system for light travel time effects. Note that the emitting shell is marked by a ring and that R denotes the distance of the line of sight away from the axis and z the distance along the line of sight.

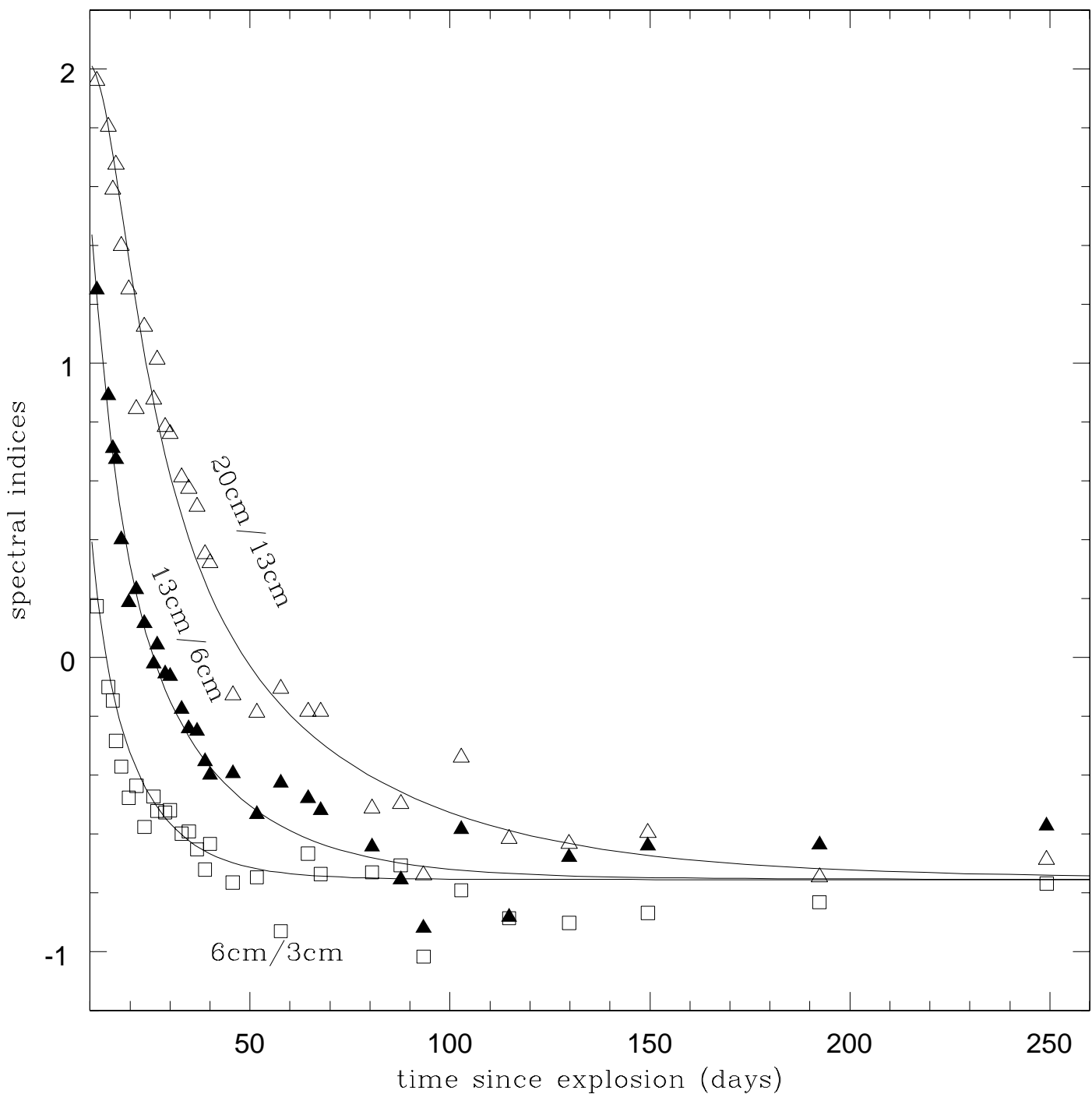
Fig. 6.— The conversion diagram for the arrival time T at the observer and the time t in the rest frame of the origin of emission from a relativistically moving shell at a given off-axis distance R . The four points, A-D, correspond to the four points in Figure 5 schematically.

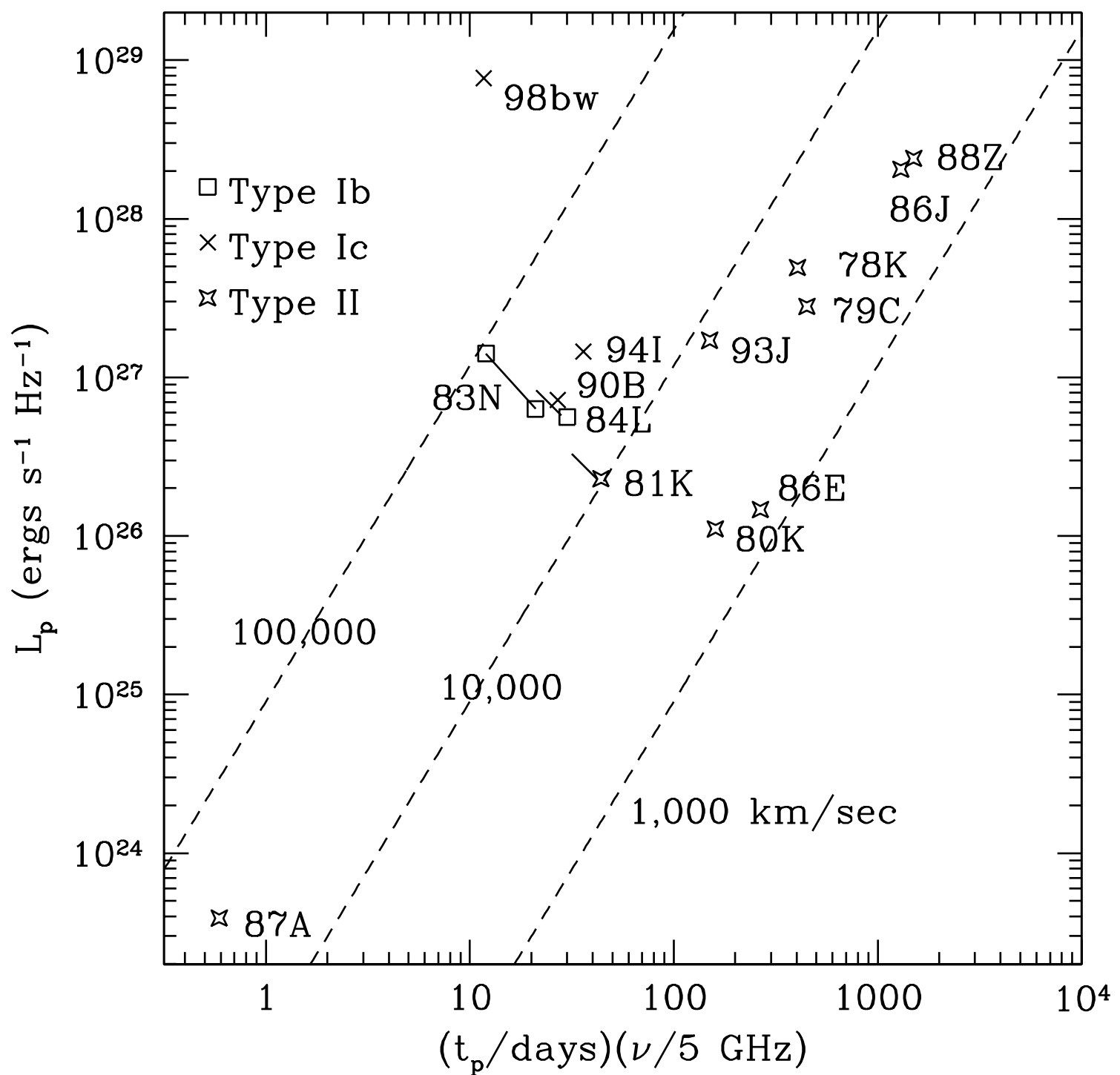
Fig. 7.— Model fits to the observed radio fluxes including dynamical and relativistic effects. Constant energy factors $\epsilon_b = \epsilon_e = 0.1$ are assumed. The second bumps in the model light curves are due to a sudden jump in the total energy (to about 2.8 times its initial value).

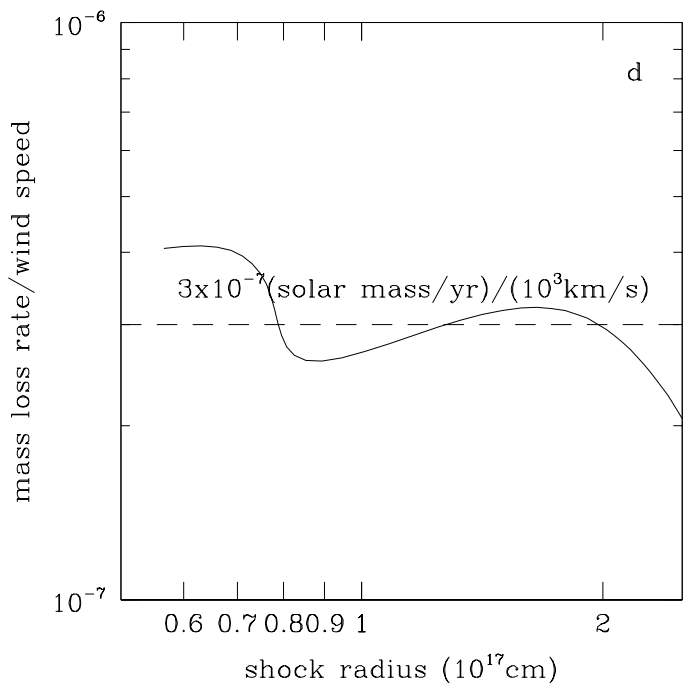
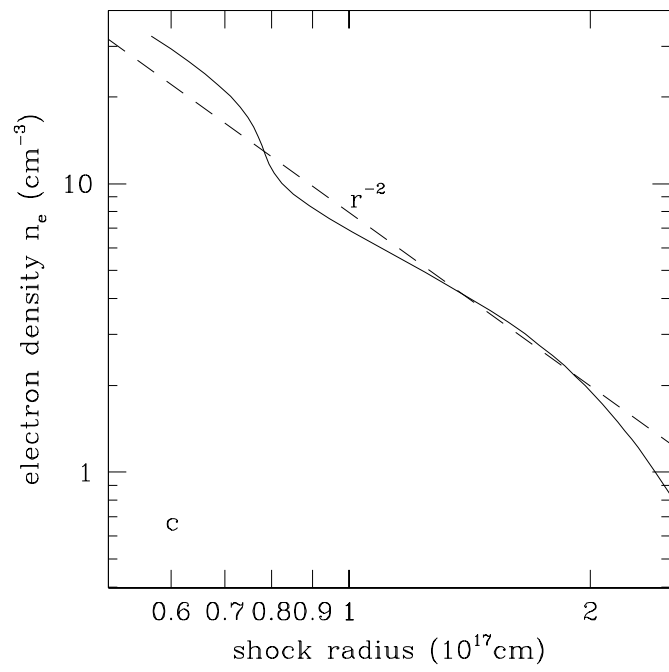
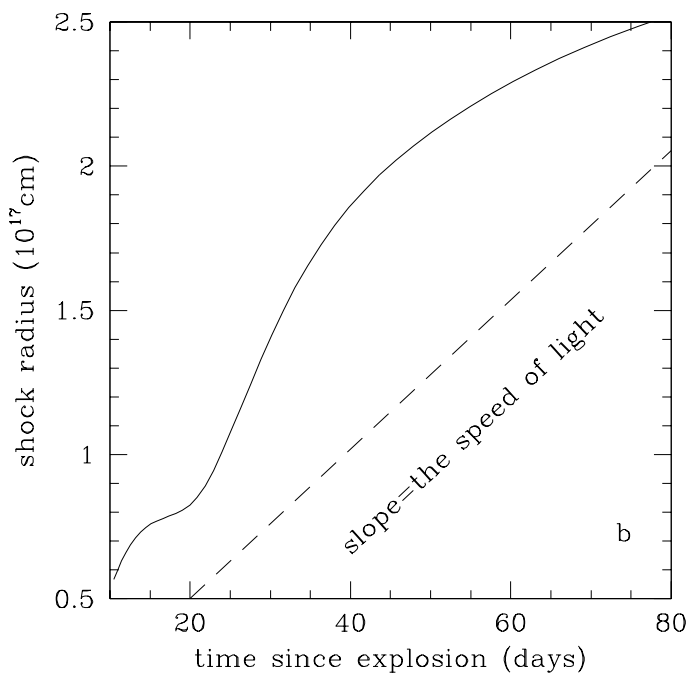
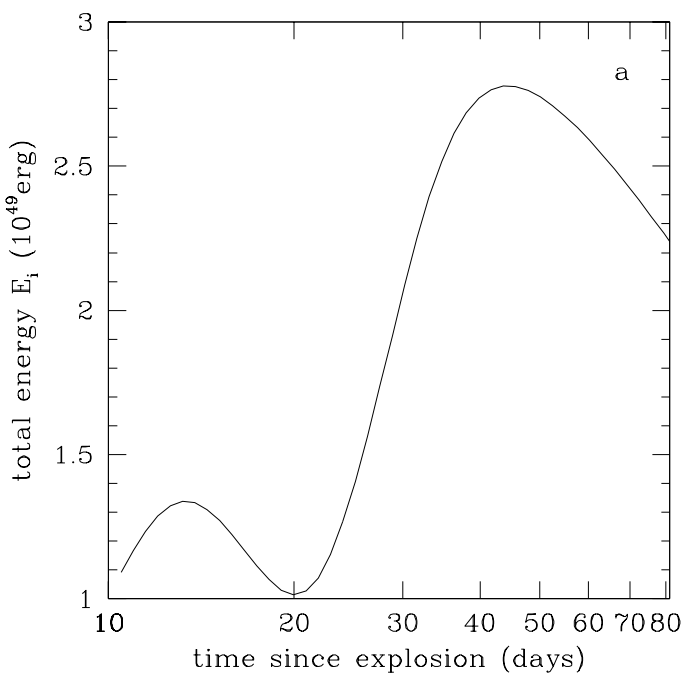
Fig. 8.— Time evolution of the shock speed. The jump is caused by the jump in the total energy. The transrelativistic nature of the blast wave is evident.

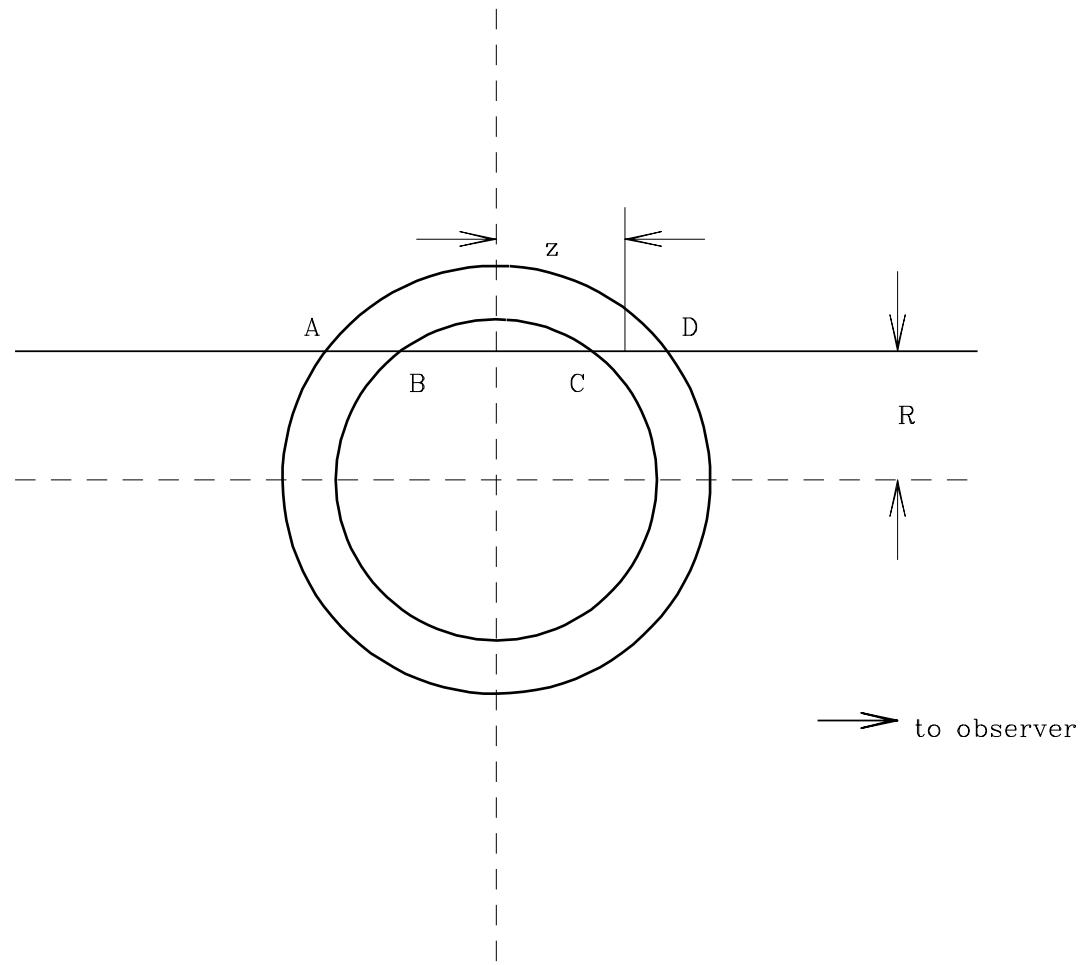
Fig. 9.— Model fits to the observed radio fluxes including dynamical and relativistic effects in the case of a magnetic energy factor $\epsilon_b = 10^{-6}$ and an electron energy factor $\epsilon_e = 1$. See Figure 7 for comparison.



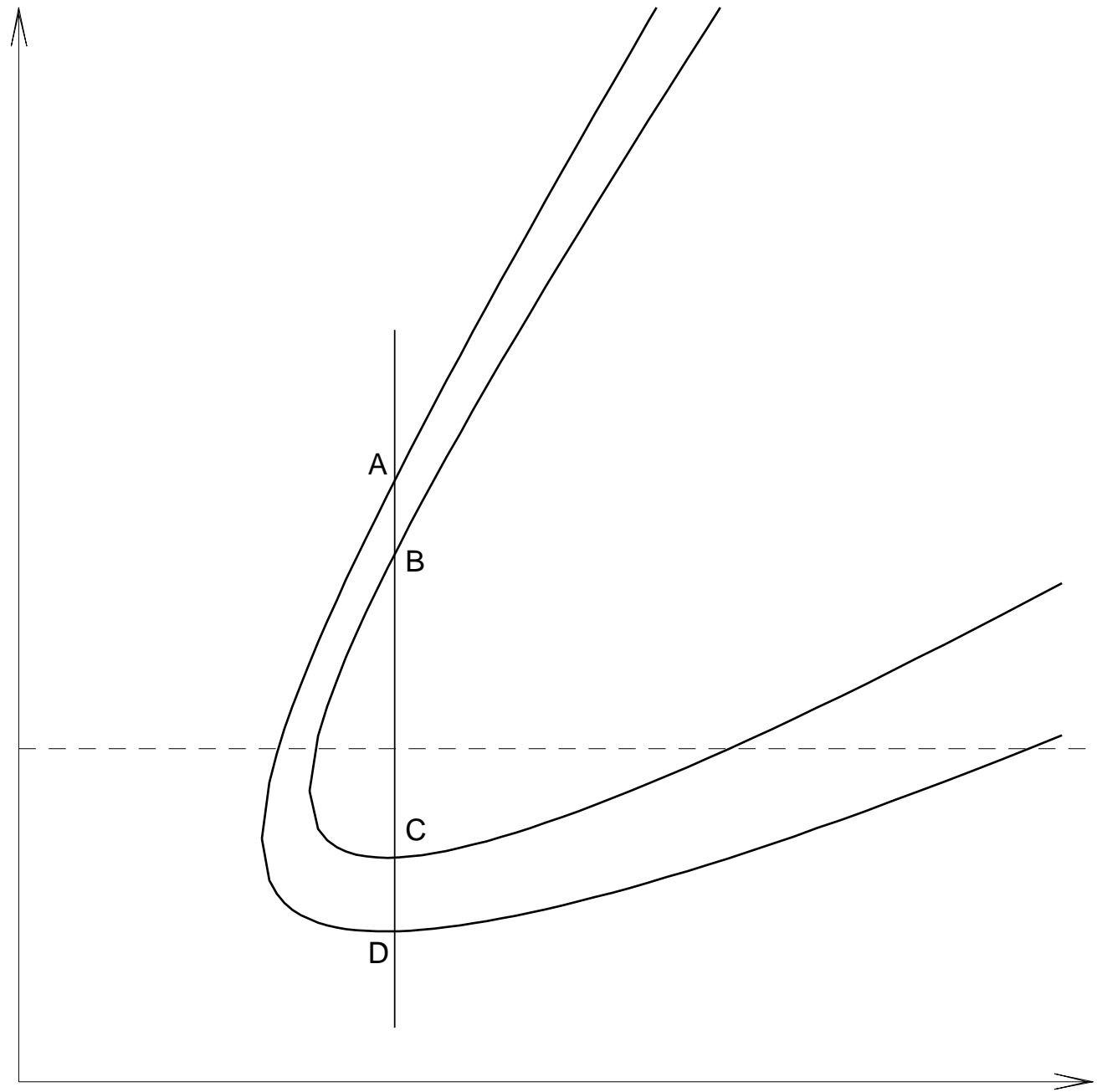








arrival time T at the observer



emission time t in the rest frame of the origin

